A PRELIMINARY ANALYSIS OF UCSB'S SOUTH POLE 1993-94 RESULTS

J. GUNDERSEN, M. LIM, J. STAREN, N. FIGUEIREDO, T. GAIER
T. KOCH, P. MEINHOLD, M. SEIFFERT, G. COOK, P. LUBIN
Department of Physics, University of California
Santa Barbara, CA 93106-9530, USA
and the Center for Particle Astrophysics, University of California

and

A. WUENSCHE
Departamento de Astrofisica, INPE/MCT
São José dos Campos, SP, Brasil 12200

ABSTRACT

We report on our continuing efforts to measure degree-scale anisotropy in the Cosmic Microwave Background. We performed three observations using the Advanced Cosmic Microwave Explorer telescope and two different broad band High Electron Mobility Transistor based receivers operating at seven frequencys between 26 and 45 GHz. The data presented here show the first two observations with the 38-45 GHz system which operated for 200 hours between January 1, 1994 and January 15, 1994 at the Amundsen-Scott South Pole Station. These two data sets show a statistically significant, correlated signal which appears to be celestial in origin.

1. Introduction

Anisotropy measurements of the cosmic microwave background (CMB) provide an effective method for testing cosmic structure formation models. In particular degree-scale anisotropy measurements can be powerful in constraining scenarios of large scale structure formation and values of global parameters in cosmic evolution models[1] and perhaps can be used to discriminate between Gaussian and non-Gaussian structure formation models[2]. Over the past five years, our group has travelled to the South Pole to perform degree scale anisotropy measurements. The results from these measurements are detailed in references 3 and 4 for our 1988-89 measurements (SP89) and references 5 and 6 for our 1990-91 measurements (SP91). We report here on our most recent measurements which occurred in 1993-94 (SP93).

2. The Experiment

All of the SP93 observations used the Advanced Cosmic Microwave Explorer (ACME) which is a one meter F1 off axis Gregorian telescope[4]. During these observations the nutating ellipsoidal secondary oscillated sinusoidally at 8 Hz with a peak to peak throw of 3° on the sky. The receiver signals were then phase synchronous

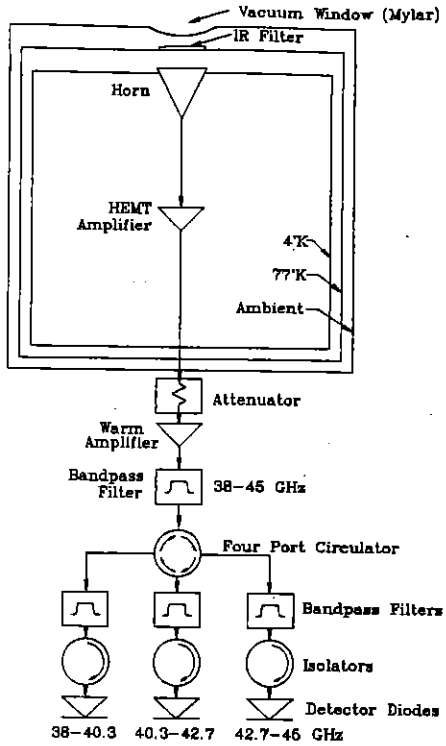
Vacuum Window (Mylar)
IR Filter
Horn
HEMT Amplifier
4°K
77°K
Ambient
Attenuator
Warm Amplifier
Bandpass Filter
38–45 GHz
Four Port Circulator
Bandpass Filters
Isolators
Detector Diodes
38–40.3
40.3–42.7
42.7–46 GHz

demodulated using a "square wave" lockin amplifier which gave a maximum sensitivity to signals separated by 2.1° on the sky.

The 26-36 GHz (Ka-band) receiver is very similar to the receiver shown in Gaier et al.[5] This receiver incorporates a very low noise, cryogenic High Electron Mobility Transistor (HEMT) amplifier[7] built at the National Radio Astronomy Observatory (NRAO). The full 10 GHz band is multiplexed into four channels, each with 2.5 GHz nominal bandwidth. This band subdivision is used to compensate for gain variations across the full band and to obtain spectral information which can be used to discriminate between the various astrophysical foregrounds shown in Figure 2. The beam profile of the telescope can be estimated with as a Gaussian beam with a full width at half maximum (FWHM) which varied between 1.4° for the highest frequency channel to 1.8° for the lowest frequency channel.

Figure 1. Q-band receiver schematic.

The 38-45 GHz (Q-band) receiver, shown in Figure 1, uses a cryogenic HEMT amplifier which is based on an NRAO design and built at UCSB. This amplifier uses an AlInAs/GaInAs/InP HEMT[8] in the first stage of amplification. This new InP based HEMT technology provided for the very low (10-15 K) receiver temperature and also requires significantly less power than the GaAs HEMTs. As with the Ka-band receiver, the Q-band system was multiplexed into 3 frequency bands with nominal bandwidths of 2.3 GHz as shown if Figure 1. With the addition of the Q-band system, our frequency coverage has doubled from our SP91 results and should allow for much improved foreground discrimination. The beam size of the Q-band receiver varies from 1.0° in the highest frequency channel to 1.2° in the lowest

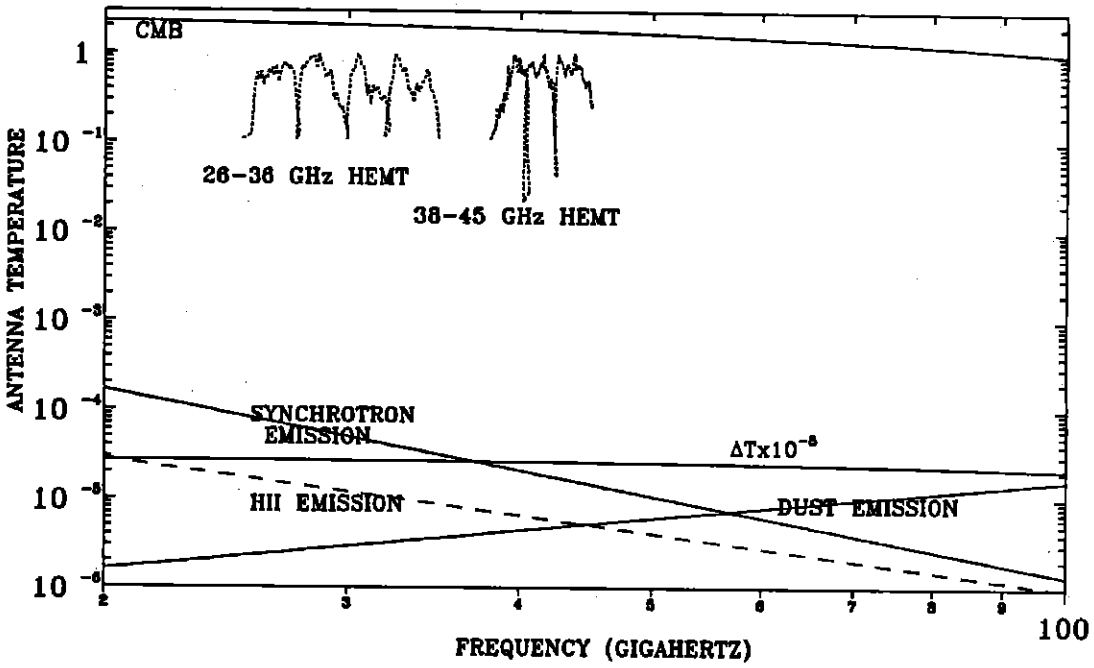
CMB
1
10^{-1}
10^{-2}
10^{-3}
10^{-4}
10^{-5}
10^{-6}
ANTENNA TEMPERATURE
26-36 GHz HEMT
38-45 GHz HEMT
SYNCHROTRON EMISSION
$\Delta T \times 10^{-6}$
HII EMISSION
DUST EMISSION
2
3
4
5
6
7
8
9
100
FREQUENCY (GIGAHERTZ)

frequency channel.

Figure 2. Estimates of high galactic latitude differential emission from galactic contaminants. Also shown are the normalized bandpasses of the Ka and Q band receivers.

3. Observation Strategy

The observation strategy was constrained by terrestial foregrounds, astrophysical foregrounds and previous observations. In order to minimize sidelobe response from the Earth and an excessive increase in the system temperature from the Earth's atmosphere, our CMB observations were limited to high elevations (large negative declinations at the South Pole). Typically, we have chosen an elevation greater than 60°. The astrophysical foregrounds in addition to the Sun tend to be more constraining in terms of observation strategies. We have used the 408 MHz Haslam map[9], the 100 micron IRAS map[10], and the Kuhr catalogue[11] of 1 Jy sources at 5 GHz to choose a region which is relatively free from synchrotron, dust and discrete radio source contamination. The sky coverage for SP93 is shown as boxes in Figure 3 along with the best estimate for the sky coverage for SP91 shown as FWHM circles. The first observation extended to ±10° on the sky about the fiducial $\alpha = 32°$ at a $\delta = -61.25°$. The second and third observations extended to ±10° on the sky about the fiducial $\alpha = 45°$ at a $\delta = -62°$. The boxes in Figure 3 represent the fact that the SP93 observations utilized smooth scans in azimuth as opposed to stepped scans for SP89 and SP91. The smooth scans have three distinct advantages over stepped

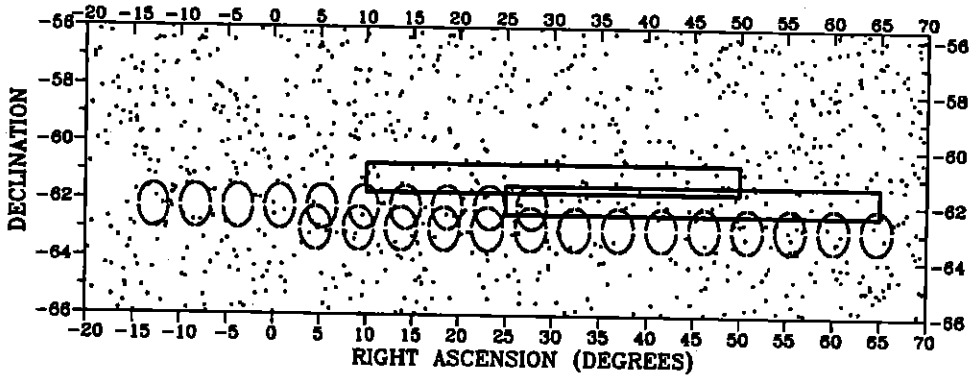
DECLINATION
RIGHT ASCENSION (DEGREES)
-56
-58
-60
-62
-64
-66
-20 -15 -10 -5 0 5 10 15 20 25 30 35 40 45 50 55 60 65 70

scans. First, a complete scan (e.g. moving the beam from α=12° to an α=52° and back to α=12°) can be performed in less than half the time it took a comparable scan in SP91. Secondly, the smooth scans afford better discrimination against unresolved sources, and third, the smooth scans increased the sky coverage while reducing the per pixel sensitivity. The relative offset in right ascension (between SP91 and SP93) was intentionally performed in order to reduce the sidelobe contamination from the Sun as observed in SP91[6]. The relative offset of 1 degree in declination was unintentional and was only discovered after the first Q-band observation. No correction was made in the other two observations.

During the CMB observations, the closest approach to the Sun was 66° on the sky and the closest approach to the plane of the galaxy occurred at a galactic latitude of −40° and a galactic longitude of 272°. In addition to CMB anisotropy measurements, we made a map of the Eta Carinae nebula and the Moon. These two measurements are very useful in checking our cold load calibrations, our absolute pointing and our beam sizes and shape. A detailed discussion of these two measurements will await a future publication. We also performed measurements of the atmospheric temperature as a function of elevation and atmospheric stability. Daily calibrations were performed by inserting an ambient black body target into the beam. These calibrations varied by less than a few percent over the 15 days of observing.

Figure 3. Sky coverage for SP91 and SP93. The ellipses represent the projected FWHM of the Ka-band receiver from our SP91 stepped scan observations. The rectangles represent the sky coverage from our two SP91 Q-band observations. The points represent the discrete radio sources from the PMN survey which is a complete listing of sources with flux densities larger than 25 mJy at 4.85 GHz.

4. Data Reduction and Analysis

We removed data when the telescope was not pointed in the correct direction, when the telescope was being serviced, when the secondary modulation was poor, when there was radio frequency interference, and when the weather made it impossible to observe. These combined effects rendered roughly 25 percent of the data

unusable. Following the analyses of Gaier et al.[5] and Schuster et al.[6], we removed an offset and linear gradient as a function of time from each half scan. The resulting data sets for the first and second observations of the Q-band system are shown in Figures 4. The mean and variance is calculated for each of the 43 bins, and the $\pm$ 1 σ error is shown in Figure 4. Each of these bins subtends an angle of 0.465° on the sky. There is a statistically significant signal in the first observation with $\chi^2/41 = 3.2$, 2.0, and 3.0 for the 39, 41, and 43 GHz channels, respectively. The second observation has a smaller, yet statistically significant signal with $\chi^2/41 =$ 1.5, 2.3, and 2.2 for the 39, 41, and 43 GHz channels, respectively. The structure appears to be quite well correlated between the channels for each observation, and the structure is somewhat correlated between the two observations though they are separated by 3/4 of a FWHM in declination.

In order to test for foreground contamination from the Sun and Earth, the data was binned into heliocentric and geocentric coordinates. For each of the two observations described above, the Sun moved about 7° with respect to the scan center. Thus, if there was any contamination due to the Sun, it would have an increased signal when binned in heliocentric coordinates. We find that the signal decreases when the binned in heliocentric coordinates, and thus conclude that the observed signal is most likely not due to the Sun. Likewise, the data was binned into geocentric coordinates (azimuth and elevation) and no significant structure was observed. As a second check for terrestial contamination, each of the two observations were split into four parts depending on which azimuthal quadrant the beam was pointed. The data was then binned into (α, δ) coordinates and compared with the complete data set. Each of the four sub-data sets were consistent with the structure observed in the complete data, although at a reduced signal to noise level. From this analysis, we can conclude that the observed structure is not due to Sun or Earth contamination.

In order to test for foreground contamination from galactic and extragalactic sources, we have made estimates of their respective contribution to the observed structure. The various foregrounds that could potentially contribute to the observed structure are thermal emission from dust, galactic synchrotron emission, galactic free-free emission, and discrete extragalactic radio sources. Using the frequency scaling given in Figure 2 and the amplitude of the dust emission in the 100 micron IRAS map, we calculate that the dust would contribute less than 10 μK to the measured rms. Likewise, for synchrotron emission, we use the scaling given in Figure 2 and the amplitude of the emission in the 408 MHz Haslam map to calculate that synchrotron emission would contribute less than 10 μK to the measured rms. Since there are no direct measurements of free-free emission in this region, we can only estimate this contribution by assuming all of the emission in the 408 MHz map is due to free-free emission and scaling the measured antenna by $\nu^{-2.1}$ to our frequencies. When this is performed and our scan is simulated on the resulting map, we estimate that in the worst case, the free-free emission is a factor of 2 below the measured rms. Thus, without a more detailed spectral analysis of our own data, we cannot rule out free-free emission. The combination of the PKS[12], PMN[13], and

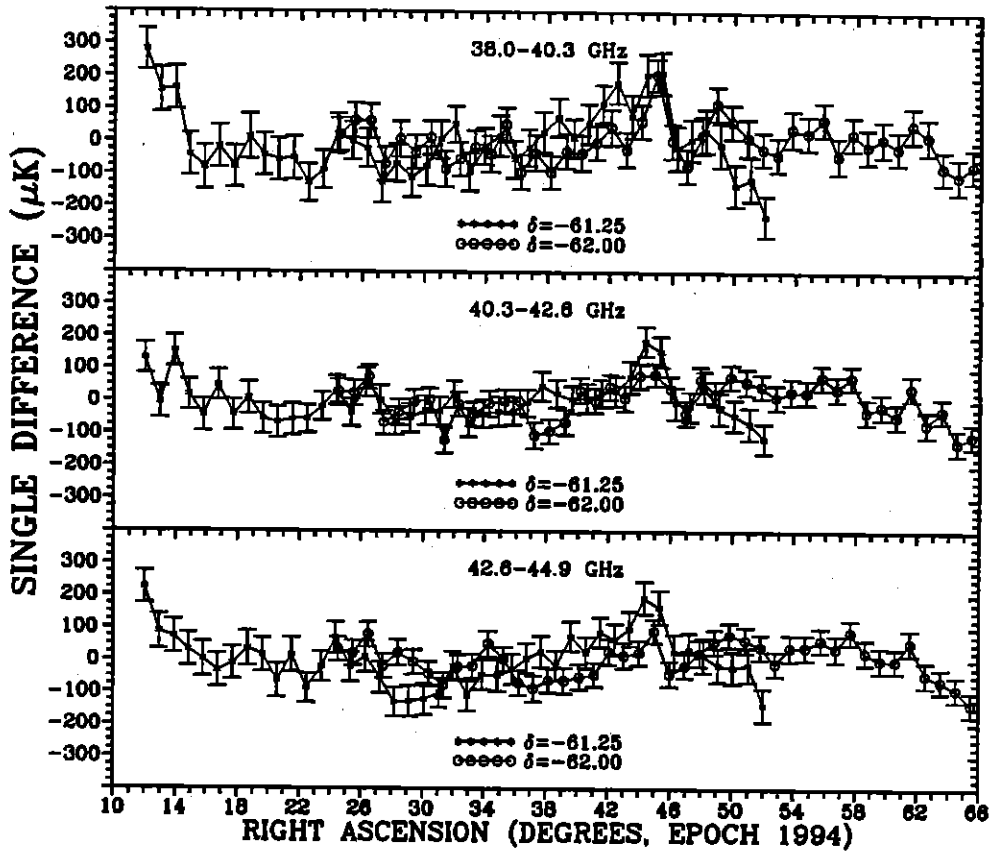
38.0-40.3 GHz
40.3-42.6 GHz
42.6-44.9 GHz
δ=-61.25
δ=-62.00
SINGLE DIFFERENCE (μK)
RIGHT ASCENSION (DEGREES, EPOCH 1994)

the Kuhr[11] catalogues allows us to estimate the foreground contribution of discrete extragalactic radio sources. For each observation there are 4 or 5 sources with enough flux density at lower frequencies, that they could contribute to the measured structure. In order for these sources to contribute to the measured struture, they would need a flat or rising spectral index (in Janskys). A flat or rising spectral index is not uncommon for these sources, so as with free-free emission, a more detailed spectral (and morphological) analysis is underway in order to determine to what extent these sources may contribute to the observed structure.

Figure 4. Single difference temperatures as measured in μK (thermodynamic) for the two Q-band observations.

5. Conclusion

We have presented further results of degree-scale anisotropy measurements of the CMB. These observations were performed at the Amundsen-Scott South Pole Station using two coherent HEMT based receivers operating at seven frequencies between 26 and 45 GHz. Significant correlated signals were observed in all bands; however, a unique source for these signals has yet to be determined. At this time, we can rule out the Earth, Sun, galactic synchrotron emission and galactic dust emission as contributors to the observed signal. A more detailed analysis is under-

way to determine whether or not free-free emission or discrete extragalactic radio sources may be contributing to the observed signal.

6. Acknowledgements

We would like to thank M. Pospieszalski, M. Balister, and W. Lakatosh of NRAO-CDL for useful information regarding amplifiers and for supplying the 26-36 HEMT amplifier. In addition we would like to thank L. Nguyen of Hughes Research Labs for providing the remarkable InP HEMTs which we've incorporated into our 38-45 GHz amplifiers. This project would have been impossible without the support of B. Sadoulet and the Center for Particle Astrophysics. D. Fischer and the whole Antarctic Support Associates staff at the Amundsen-Scott South Pole station provided the valuable assistance and expertise to get the job done. N. F. is also at Escola Federal de Engenharia de Itajubá and Instituto Nacional de Pesquisas Espaciais and was partially supported by Choshelho Nacional de Desenvolvimento Científico e Tecnolǵico, Brazil.

7. References

1. J. R. Bond et al., *Phys. Rev. Lett.* **66** (1991) 2179.
2. D. Coulson, U. Pen, and N. Turok, *Nature* (1993) submitted.
3. P. R. Meinhold and P. M. Lubin, *Ap. J.* **370** (1991) L11.
4. P. R. Meinhold et al., *Ap. J.* **406** (1993) 12.
5. T. Gaier et al., *Ap. J.* **398** (1992) L1.
6. J. Schuster et al., *Ap. J.* **412** (1993) L47.
7. M. W. Pospieszalski, J. D. Gallego, and W. J. Lakatosh, *IEEE MTT-S Digest* (1990) 1253.
8. M. W. Pospieszalski, et al., preprint, (1994).
9. C. G. T. Haslam, et al., *A&AS* **86** (1982) 1.
10. S. Wheelock et al., *IRAS Sky Survey Atlas* (1991).
11. H. Kuhr et al., *AJ* **86** (1981) 6.
12. *Parkes Catalogue* (1990) Australia Telescope National Facility.
13. P. C. Gregory et al., *ApJS* (1993) submitted.